

# $G^2$ Tensor Product Splines over Extraordinary Vertices

Charles Loop<sup>1</sup> and Scott Schaefer<sup>2</sup>

<sup>1</sup>Microsoft Research

<sup>2</sup>Department of Computer Science, Texas A&M University

---

## Abstract

We present a second order smooth filling of an  $n$ -valent Catmull-Clark spline ring with  $n$  biseptric patches. While an underdetermined biseptric solution to this problem has appeared previously, we make several advances in this paper. Most notably, we cast the problem as a constrained minimization and introduce a novel quadratic energy functional whose absolute minimum of zero is achieved for bicubic polynomials. This means that for the regular 4-valent case, we reproduce the bicubic B-splines. In other cases, the resulting surfaces are aesthetically well behaved. We extend our constrained minimization framework to handle the case of input mesh with boundary.

Categories and Subject Descriptors (according to ACM CCS): I.3.5 [Computer Graphics]: Curve, surface, solid, and object representations

---

## 1. Introduction

Catmull-Clark subdivision surfaces have become a standard modeling primitive in computer generated films and video games [CC78]. The success of this algorithm is due to its ability to model surfaces of arbitrary genus, possibly with boundary [Nas87]. The modeling paradigm is simple: a user specifies a coarse control mesh consisting of vertices, faces, and edges that approximates a desired shape; the Catmull-Clark surface smoothly approximates the control mesh in an intuitive fashion. Artists easily grasp the behavior of these shapes relative to the control mesh. However, subdivision surfaces contain shape defects at extraordinary vertices (where the number of incident edges is not equal to 4). In general the surface is only  $C^1$  at these isolated points. In entertainment scenarios, the viewpoint is controlled or the presence of isolated shape defects is acceptable. For modeling high quality shapes, subdivision surfaces are inadequate.

Subdivision surface behavior at extraordinary vertices has been extensively studied and their shape artifacts are by now well understood [DS78, Rei95, PR98, Pra98, RS99]. Tangent plane continuity at extraordinary vertices was formally established in [Rei95]. However, no modification to the subdivision rules will result in curvature continuity at these points [Pra98]. Modifications that bound the otherwise unbounded curvature at extraordinary vertices have appeared [Sab91, ADS06, GU07]. A weak form of curvature continu-

ity has been achieved by locally projecting the control mesh to a flat spot with zero curvature [Rei98, PU98]. True curvature continuity has been obtained by blending a disk shaped region about the extraordinary vertex with a quadratic shape [Zor06, Lev06]. All of these schemes are concerned with the limiting behavior of the subdivision process, and not the removal of the underlying singularities in the mapping from a manifold domain to an embedding space.

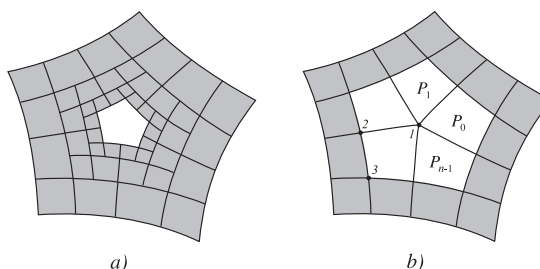


**Figure 1:** a) Each subdivision step adds a new spline ring to the interior of the hole created by an extraordinary vertex. b) The work presented in this paper fills the hole in a Catmull-Clark spline ring with  $n$  biseptric patches  $P_0, \dots, P_{n-1}$ . Examples of vertex types 1, 2, and 3 are also shown.

These singularities, corresponding to the extraordinary vertices of the control mesh, are a result of the inherently

functional spline machinery used by many subdivision algorithms. That is, Catmull-Clark surfaces are bicubic tensor product B-splines, albeit over procedurally defined control meshes with infinite structure. Such a componentwise functional spline is a deformation of a regular planar lattice, so modeling an arbitrary genus surface with a more general tessellation requires singularities. This fact is invariably ignored in the theoretical study of extraordinary vertex behavior under subdivision. Instead that study focuses on so-called *spline rings*, a local collection of surface patches that form an  $n$ -sided hole about an extraordinary vertex, see Figure 1a. As subdivision proceeds, a new spline ring is formed inside the hole such that the old and new spline rings join with the smoothness of the underlying B-spline. In the limit, the  $n$ -sided hole becomes infinitesimally small, but never vanishes. This infinite set of polynomials and the limiting behavior at extraordinary vertices complicates evaluation and processing of these surfaces [HKD93, Sta98] whereas surfaces composed of a finite set of polynomials are substantially simpler.

### 1.1. Problem Statement and Contributions

The problem we address can be reduced to the following:

*Fill the hole in an  $n$ -valent Catmull-Clark spline ring with  $n$  tensor product patches that join each other and the spline ring with second order smoothness.*

See Figure 1b for an illustration. Our solution to this problem requires bidegree 7 patches. This result was originally reported in [Loo04]. While that work established the existence of a biseptric solution space, ad-hoc means were used to remove the extra degrees of freedom. Here we make several improvements and contributions; specifically

1. The derivation of the underdetermined biseptric solution space is based entirely on properties of the correspondence maps between adjacent patches and the necessary cocycle condition these maps must obey about vertices.
2. Our surface is defined as a constrained minimization over a novel energy functional that achieves an absolute minimum of zero for bicubic patches and results in aesthetically pleasing shapes otherwise.
3. We solve for data independent *basis functions* explicitly, as an off-line preprocess. Since the basis functions are solved independent of the surface, we can manipulate these surfaces in realtime.
4. We define basis functions to handle meshes with boundary such that the surface interpolates the cubic B-spline curve defined by the mesh boundary.

Filling a spline ring with second order smooth surfaces has practical applications in surface design. We use our results to construct second order smooth surfaces over refined quadrilateral control meshes, where each quad has at most one incident extraordinary vertex. Refinement is needed to isolate

extraordinary vertices as is done for Catmull-Clark evaluation [Sta98]. Unlike Catmull-Clark surfaces, our surfaces are second order smooth everywhere and contain a finite number of polynomial patches.

### 1.2. Previous Work

Many papers addressing the problem of constructing first and second order smooth patch complexes have appeared over the last two decades. We mention here only those that explicitly join tensor product polynomials with second order smoothness at extraordinary vertices. In [Pra97] an  $n$ -valent Catmull-Clark spline ring is filled with bidegree 6 patches; however,  $4n$  such patches are needed. Similarly, [GZ99] form a second order smooth join over extraordinary vertices with  $4n$  bidegree 5 patches. In [Pet02] a combination of  $2n$  bidegree  $3 \times 5$  and  $2n$  bicubic patches would be needed to fill an  $n$ -sided hole surrounded by bicubics. In [KP07], a collection  $16n$  patches of bidegree  $4 \times 4$  and  $6 \times 6$  are used to form a smooth complex surrounded by bicubic patches.

While other works have achieved lower bidegree, with respect to total control point count, bidegree 7 with  $n$  patches is still the best result. This makes the scheme attractive for GPU implementation since total data throughput is minimized. In this paper, we strive to improve shape quality, and to make the results more practically applicable.

This paper is organized as follows. In Section 2 we present aspects of geometric continuity necessary to derive our results. In Section 3 we specify the correspondence maps between adjacent patches as required by the definition of geometric continuity. In Section 4 we use the correspondence maps to derive sets of constraints on the coefficients of adjacent patches needed for second order smoothness. In Section 5 we present a novel quadratic energy functional, then show how this functional is minimized subject to our constraints in Section 6. We solve for data independent basis functions, with support and boundary constraints in Section 7. Finally, we present results and conclude with Section 8.

## 2. Geometric Continuity

Given a pair of surface patches  $P_i, P_{i+1} : [0, 1] \times [0, 1] \rightarrow \mathbb{R}^m$ , we say  $P_i$  and  $P_{i+1}$  meet with  $k^{\text{th}}$  order *geometric continuity* denoted  $G^k$  [DeR85], if there exists a map  $\theta$  such that  $P_i$  meets  $P_{i+1} \circ \theta$  with parametric continuity  $C^k$ , that is

$$P_i \stackrel{G^k}{\cong} P_{i+1} \Rightarrow P_i \stackrel{C^k}{\cong} P_{i+1} \circ \theta.$$

More formally, this condition requires that the  $k^{\text{th}}$  order derivatives of the two patches after reparameterization with respect to  $\theta$  coincide. We refer to the map  $\theta : \mathbb{R}^2 \rightarrow \mathbb{R}^2$  as the *correspondence map* between  $P_i$  and  $P_{i+1}$ . Technically  $\theta$ , along with  $k$  of its transversal derivatives, only needs to be defined on a line corresponding to the common patch boundary. However we find it convenient to define correspondence

maps in Bézier form over the entire unit square; this way transversal derivatives on edges and consistent mixed partial derivatives at vertices are easily specified.

The derivatives of  $P_{i+1} \circ \theta$  can be found via the chain rule and yield a matrix equation of the form

$$D_i = (D_{i+1} \circ \theta) \cdot \Theta$$

where  $D_i$  is a vector of the partial derivatives of  $P_i$  (i.e.  $D_i = \left[ \frac{\partial P_i}{\partial u} \quad \frac{\partial P_i}{\partial v} \quad \frac{\partial^2 P_i}{\partial u^2} \quad \dots \right]$ ) and  $\Theta$  is a matrix obtained using the chain rule that encodes the partial derivatives of  $\theta$ . We refer to  $\Theta$  as the *chain rule matrix* of  $\theta$ .

If we make the simplifying assumption that  $\theta$  is the identity function along the common boundary, then the above equation reduces to

$$D_i = D_{i+1} \cdot \Theta, \quad (1)$$

when evaluated on the boundary. This assumption is reasonable as any other choice of  $\theta$  would lead to higher degree boundary curves with more smoothness constraints. Equation 1 tells us how to transform the derivatives w.r.t. the domain of  $P_i$  in terms of the derivatives of  $P_{i+1}$  and  $\theta$ .

For a cyclic collection of  $n$  patches  $P_i$  incident on a common vertex with correspondence maps  $\theta_i$  between patches  $P_i$  and  $P_{i+1}$ ,  $i = 0, \dots, n-1$  (indices taken modulo  $n$ ), satisfying geometric continuity results in a *cocycle condition* among the patches. If we evaluate equation 1 at the common vertex for all patches, we find that

$$D_0 = D_0 \cdot \Theta_{n-1} \cdot \Theta_{n-2} \cdot \dots \cdot \Theta_1 \cdot \Theta_0,$$

for  $n$  patches incident on that vertex. Therefore, this relationship results in the additional requirement that

$$\mathbf{I} = \Theta_{n-1} \cdot \Theta_{n-2} \cdot \dots \cdot \Theta_1 \cdot \Theta_0 \quad (2)$$

when evaluated at the common vertex [Hah89]. For  $G^k$  continuity a correspondence map must encode all  $k^{th}$  order transversal derivatives in the versal direction. If we differentiate  $k$  times in this direction, will get mixed partials of order  $2k$ . These derivatives must agree at the common vertex in order to get a polynomial parameterization. Therefore, for  $G^k$  continuity the chain rule matrices must encode derivatives up to order  $2k$ .

### 3. Correspondence Maps

We will construct two types of correspondence maps on edges joining three types of vertices:

1. an extraordinary vertex,
2. an edge adjacent neighbor of a type 1 vertex,
3. a face adjacent diagonal neighbor of a type 1 vertex,

see Figure 1b. Note that a type 1 vertex is  $n$ -valent, vertex types 2 and 3 are always 4-valent. Over the edge between vertex types 1 and 2 we define *interior* correspondence maps; over the edge between vertex types 2 and 3 we define *exterior* correspondence maps.

### 3.1. Interior Correspondence Maps

We define interior correspondence maps in terms of the maps  $\phi_n : (u, v) \rightarrow (x, y)$  defined by

$$\begin{aligned} \phi_{n,x}(u, v) &= \mathbf{b}^1(u)^T \begin{bmatrix} 0 & \cos\left(\frac{2\pi}{n}\right) \\ 1 & 1 \end{bmatrix} \mathbf{b}^1(v), \\ \phi_{n,y}(u, v) &= \mathbf{b}^1(u)^T \begin{bmatrix} 0 & \sin\left(\frac{2\pi}{n}\right) \\ 0 & \tan\left(\frac{\pi}{n}\right) \end{bmatrix} \mathbf{b}^1(v), \end{aligned}$$

where  $\mathbf{b}^d(\cdot)$  are degree  $d$  Bernstein polynomials. The geometry of  $\phi_n$  is illustrated in Figure 2.1. Given that  $\phi_n$  creates an angle of  $\frac{2\pi}{n}$  around the extraordinary vertex, the correspondence map from patch  $P_i$  to  $P_{i+1}$  is  $\phi_n^{-1} \circ (r_n^{-1} \circ \phi_n)$  where  $r_n$  is a counterclockwise rotation of  $\frac{2\pi}{n}$  about the origin.

We verify the cocycle condition at a type 1 vertex using the chain rule matrices  $\Phi_n$  and  $R_n$  for  $\phi_n$  and  $r_n$  respectively. We form the composition of the correspondence maps  $(\phi_n^{-1} \circ r_n^{-1} \circ \phi_n)$  from patches 0 through  $n-1$  and evaluate at  $(0, 0)$ , corresponding to the extraordinary vertex to get

$$\mathbf{I} = \left( \Phi_n^{-1} \cdot R_n^{-1} \cdot \Phi_n \right)^n = \Phi_n^{-1} \cdot \left( R_n^{-1} \right)^n \cdot \Phi_n.$$

Notice that  $(R_n^{-1})^n = \mathbf{I}$  because  $r_n^{-1}$  is a rotation of  $\frac{2\pi}{n}$ . The above expression only depends on  $\Phi_n$  being locally invertible at  $(0, 0)$ . The cocycle loop of correspondence maps incident on a type 1 vertex is illustrated in Figure 2.1.

### 3.2. Exterior Correspondence Maps

The second type of correspondence map we need is defined over an edge between vertex types 2 and 3; this edge corresponds to the boundary of the spline ring. Unlike the interior correspondence maps, we must carefully solve for the exterior correspondence maps. In previous work [Loo04] the same correspondence maps were derived by appealing to the embedding space of the resulting patches. Here we derive the correspondence maps strictly in terms of abstract adjacency relations of the underlying tessellation.

We begin by defining maps  $\psi_n : (u, v) \rightarrow (x, y)$ , where  $n$  is the valence of the nearby extraordinary vertex. The exterior correspondence maps will be defined by  $\psi_n(u, 1)$  and  $\psi_n(1, v)$ , where  $u, v \in [0, 1]$ . We require  $\psi_n$  to be the identity on the edges  $(u, 0)$ ,  $(u, 1)$ ,  $(0, v)$ , and  $(1, v)$ . Parameter values  $(1, 0)$  and  $(0, 1)$  correspond to type 2 vertices;  $(1, 1)$  corresponds to the type 3 vertex. Figure 2.2 illustrates the cocycle loop where four patches meet at a type 2 vertex. Note that this vertex might share an edge with another extraordinary vertex of valence  $m$ , which is possible given the minimum separation of extraordinary vertices we require. We can factor the cocycle composition into two parts, corresponding to

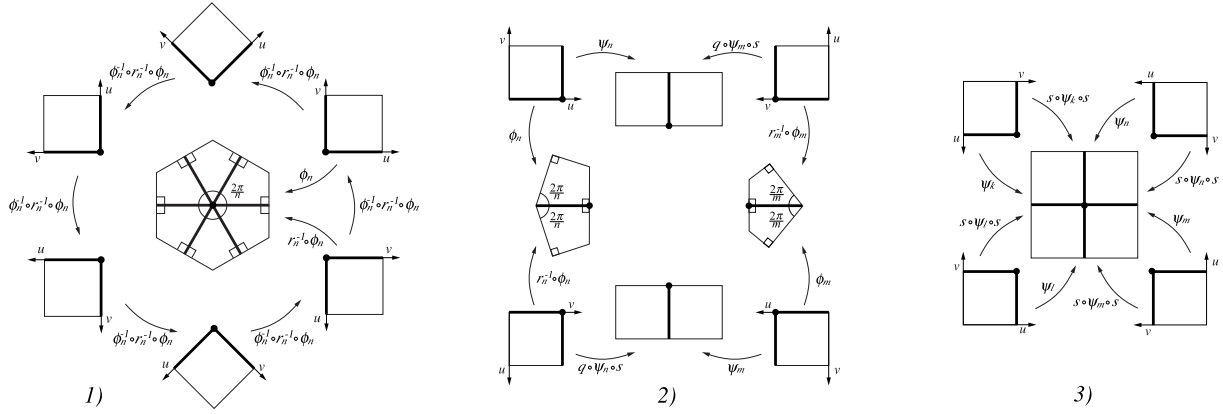


**Figure 2:** The cocycle maps for the 3 vertex types : 1) extraordinary vertex, 2) edge sharing neighbor of a type 1 vertex 3) face sharing diagonal neighbor of a type 1 vertex

the two neighboring extraordinary vertices to get

$$\mathbf{I} = \underbrace{Q \cdot \Psi_n \cdot S \cdot (R_n^{-1} \cdot \Phi_n)^{-1} \cdot \Phi_n \cdot \Psi_n^{-1}}_{\mathbf{I}} \cdot \underbrace{Q \cdot \Psi_m \cdot S \cdot (R_m^{-1} \cdot \Phi_m)^{-1} \cdot \Phi_m \cdot \Psi_m^{-1}}_{\mathbf{I}}, \quad (3)$$

where  $Q$  is the chain rule matrix for  $q(u, v) = (u, -v)$  the reflection across the  $u$  axis,  $S$  is the chain rule matrix for  $s(u, v) = (v, u)$  the reflection across the diagonal  $u = v$ ,  $R_n$  is the chain rule matrix for a  $\frac{2\pi}{n}$  rotation about the origin, and  $\Psi_n$  is the chain rule matrix for  $\psi_n$ . Note that parameter for evaluation of these matrices corresponds to the type 2 vertex. Both factors of equation 3 represent the identity and are the same up to valence. The factor involving  $n$  will impose constraints of various partial derivatives on  $\psi_n$  at the type 2 vertex.

Additional constraints on  $\psi_n$  come from the cocycle condition at the type 3 vertex. Figure 2.3 illustrates the cocycle loop where four patches meet at a type 3 vertex. We assume that this vertex may be a diagonal neighbor of four extraordinary vertices. By assuming the symmetry  $\psi_n(u, v) = \psi_n(v, u)$ , the cocycle composition at a type 3 vertex can be factored into four parts, corresponding to the 4 arbitrary valence diagonal neighbors

$$\mathbf{I} = \underbrace{\Psi_k \cdot (S \cdot \Psi_k \cdot S)^{-1}}_{\mathbf{I}} \cdot \underbrace{\Psi_\ell \cdot (S \cdot \Psi_\ell \cdot S)^{-1}}_{\mathbf{I}} \cdot \underbrace{\Psi_m \cdot (S \cdot \Psi_m \cdot S)^{-1}}_{\mathbf{I}} \cdot \underbrace{\Psi_n \cdot (S \cdot \Psi_n \cdot S)^{-1}}_{\mathbf{I}}. \quad (4)$$

This expression holds since  $S \cdot \Psi_n \cdot S = \Psi_n$ .

We use the constraints imposed on the derivatives of  $\psi_n$

by equations 3 and 4 to find  $\psi_{n,x}(u, v) =$

$$\mathbf{b}^4(u)^T \begin{bmatrix} 0 & 0 & 0 & 0 \\ \frac{1}{4} & \frac{5c_n^2 - 3c_n - 15c_n + 18}{12(c_n - 2)(2c_n - 3)} & \frac{c_n^2 + 2c_n - 6}{12(c_n - 2)} & \frac{1}{4} \\ \frac{1}{2} & \frac{c_n + 3}{6} & \frac{c_n^2 + 3c_n - 9}{9(c_n - 2)} & \frac{1}{2} \\ \frac{3}{4} & \frac{c_n + 9}{12} & \frac{c_n + 9}{12} & \frac{3}{4} \\ 1 & 1 & 1 & 1 \end{bmatrix} \mathbf{b}^3(v),$$

where  $c_n = \cos(\frac{2\pi}{n})$ . By the symmetry condition, we also have  $\psi_{n,y}(u, v) = \psi_{n,x}(v, u)$ . The derivation of this solution is presented in Appendix A. Note that when  $n = 4$ ,  $\psi_4 = \mathbf{I}$ .

#### 4. Patch Smoothness Constraints

We now use the correspondence maps to determine second order smoothness constraints on the coefficients of the patches  $P_i, i = 0, \dots, n - 1$ .

##### 4.1. External Constraints

A Catmull-Clark spline ring surface is completely characterized by a 3-ring of points about an extraordinary vertex. However, the second order behavior of the spline ring boundary can be described by a 2-ring. We label the points of this 2-ring in a cyclic fashion, as shown in Figure 3. Note that we have  $n$  seven point sections and the central vertex is duplicated  $n$  times; doing so will give us a circulant system of equations in Section 4.3.

We characterize the second order behavior of the spline ring boundary with a set of  $n$  bicubic patches. The control points of these bicubic Bézier patches are found by applying the cubic knot insertion operator

$$\mathbf{M} = \frac{1}{6} \begin{bmatrix} 1 & 0 & 0 & 0 \\ 4 & 4 & 2 & 1 \\ 1 & 2 & 4 & 4 \\ 0 & 0 & 0 & 1 \end{bmatrix},$$

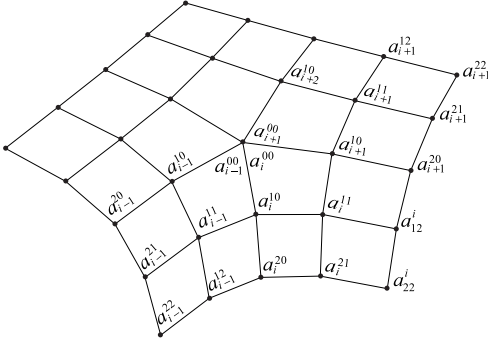


Figure 3: A 2-ring  $a$  with point labeling.

on the 2-ring control points. This will convert from B-spline to Bernstein form resulting in  $n$  bicubic Bézier patches

$$H_i(u, v) = \mathbf{b}^3(u)^T \mathbf{M}^T \begin{bmatrix} \cdot & a_{i+2}^{10} & a_{i+1}^{11} & a_{i+1}^{21} \\ a_{i-1}^{10} & a_i^{00} & a_{i+1}^{10} & a_{i+1}^{20} \\ a_{i-1}^{11} & a_i^{10} & a_i^{11} & a_i^{12} \\ a_{i-1}^{12} & a_i^{20} & a_i^{21} & a_i^{22} \end{bmatrix} \mathbf{M} \mathbf{b}^3(v),$$

where  $i = 0, \dots, n-1$  and  $a_i^{jk}$  are control mesh vertices from Figure 3. Note that, due to the undefined control point (represented by a "." above), the patches  $H_i$  can only be evaluated along the external boundary  $(u, 1)$  and  $(1, v)$ ; however, all derivatives up to second order are well defined on this boundary. Furthermore, these derivatives will meet the surrounding spline ring with  $C^k$  continuity.

Next, we use the maps  $\psi_n$  from Section 3.2 to reparameterize the bicubic patches  $H_i$  to get constraints on the external edge of our patches; that is

$$\frac{\partial^j}{\partial u^j} P_i(1, t) = \frac{\partial^j}{\partial u^j} (H_i \circ \psi_n)(1, t), \quad j = 0, 1, 2.$$

Expanding this expression using the chain rule results in the following external constraints on patch  $P_i$

$$P_i(1, t) = H_i(1, t), \quad (5)$$

$$\begin{aligned} \frac{\partial}{\partial u} P_i(1, t) &= \frac{\partial}{\partial x} H_i(1, t) \frac{\partial}{\partial u} \psi_{n,x}(1, t) \\ &+ \frac{\partial}{\partial y} H_i(1, t) \frac{\partial}{\partial u} \psi_{n,y}(1, t), \end{aligned} \quad (6)$$

$$\begin{aligned} \frac{\partial^2}{\partial u^2} P_i(1, t) &= \frac{\partial}{\partial x} H_i(1, t) \frac{\partial^2}{\partial u^2} \psi_{n,x}(1, t) \\ &+ \frac{\partial}{\partial y} H_i(1, t) \frac{\partial^2}{\partial u^2} \psi_{n,y}(1, t) \\ &+ \frac{\partial^2}{\partial x^2} H_i(1, t) \left( \frac{\partial}{\partial u} \psi_{n,x}(1, t) \right)^2 \\ &+ 2 \frac{\partial^2}{\partial xy} H_i(1, t) \frac{\partial}{\partial u} \psi_{n,x}(1, t) \frac{\partial}{\partial u} \psi_{n,y}(1, t) \\ &+ \frac{\partial^2}{\partial y^2} H_i(1, t) \left( \frac{\partial}{\partial u} \psi_{n,y}(1, t) \right)^2. \end{aligned} \quad (7)$$

The constraints along the boundary  $(t, 1)$  are defined similarly. All terms on the right hand sides of Equations 5, 6,

and 7 are polynomials of known degree. From this, we can deduce by degree counting, that the patches  $P_i$  must be bidegree 7.

To determine the number of constraints given by equations 5, 6, and 7, we note that each of these 3 equations is a degree 7 polynomial with 8 degrees of freedom resulting in 24 constraints. Therefore we have 48 constraints for both edges of the external boundary. However, at  $u = v = 1$  (corresponding to a type 3 vertex), the cocycle condition guarantees that the mixed partial derivatives will agree up to second order, meaning that 9 of these constraints will be dependent; so there are only 39 external constraints per patch, or  $39n$  for all patches sharing the type 1 vertex.

## 4.2. Internal Constraints

We now derive constraints along internal patch edges. We combine the internal correspondence map  $(\phi_n^{-1} \circ r_n^{-1} \circ \phi_n)$  between the pair of surface patches  $P_i(0, t)$  and  $P_{i+1}(t, 0)$ , with the definition of second order geometric continuity to get the relation

$$\frac{\partial^{j+k}}{\partial u^j \partial v^k} P_i(0, t) = \frac{\partial^{j+k}}{\partial u^j \partial v^k} \left( P_{i+1} \circ \phi_n^{-1} \circ r_n^{-1} \circ \phi_n \right) (t, 0)$$

where  $j+k = 0, 1, 2$ . Expanding this gives us  $G^0$ ,  $G^1$  and  $G^2$  constraints

$$P_i(0, t) = P_{i+1}(t, 0), \quad (8)$$

$$\begin{aligned} c_n(1-t) \left( \frac{\partial}{\partial u} P_{i+1}(t, 0) + \frac{\partial}{\partial v} P_i(0, t) \right) &= \\ \left( \frac{\partial}{\partial v} P_{i+1}(t, 0) + \frac{\partial}{\partial u} P_i(0, t) \right), \end{aligned} \quad (9)$$

$$\begin{aligned} 2c_n^2(1-t) \left( \frac{\partial}{\partial v} P_{i+1}(t, 0) - \frac{\partial}{\partial u} P_i(0, t) \right) &+ \\ 2c_n(1-t)(1+c_n(1-t)) \left( \frac{\partial^2}{\partial uv} P_{i+1}(t, 0) - \frac{\partial^2}{\partial uv} P_i(0, t) \right) &= \\ (1+c_n(1-t)) \left( \frac{\partial^2}{\partial v^2} P_{i+1}(t, 0) - \frac{\partial^2}{\partial u^2} P_i(0, t) \right). \end{aligned} \quad (10)$$

We count the number of constraints determined by these equations as follows. Since patches  $P_i$  are biseptic, we can deduce (by degree counting) the number of constraints in equations 8, 9, and 10, are 8, 8, and 9 respectively; therefore we have 27 constraints per internal edge. However, the external constraints derived in the previous section specify the 9 second order mixed partial derivatives corresponding to the type 2 vertex at  $P_{i+1}(1, 0)$  and  $P_i(0, 1)$ . By the cocycle condition, these derivatives will automatically satisfy 8, 9, and 10 resulting in 9 dependent constraints. Therefore the geometric continuity conditions introduce  $16n$  internal constraints.

## 4.3. Constraint System

The  $16n$  internal constraints combined with the  $39n$  external constraints results in a system of  $55n$  equations. Each biseptic patch  $P_i$  has 64 coefficients, so we have a system of  $55n$

equations in  $64n$  unknowns. All of our constraints are polynomial equations that can be written in terms of biseptic Bézier control points  $p_i^{jk}$  and two-ring control mesh vertices  $a_i^{lm}$ . We can write the constraints as a block circulant system

$$\mathbf{Cp} = \mathbf{W}\mathbf{a}, \quad (11)$$

that expands to

$$\begin{bmatrix} \mathbf{c}_0 & \mathbf{c}_1 & \cdots & \mathbf{0} \\ \mathbf{0} & \mathbf{c}_0 & & \vdots \\ \vdots & & \ddots & \mathbf{0} \\ \mathbf{c}_1 & \cdots & \mathbf{0} & \mathbf{c}_0 \end{bmatrix} \begin{bmatrix} p_0 \\ p_1 \\ \vdots \\ p_{n-1} \end{bmatrix} = \begin{bmatrix} \mathbf{w}_0 & \mathbf{w}_1 & \cdots & \mathbf{w}_{n-1} \\ \vdots & \vdots & \ddots & \vdots \\ \mathbf{w}_{n-1} & \mathbf{w}_0 & & \vdots \\ \vdots & \vdots & \ddots & \mathbf{w}_1 \\ \mathbf{w}_1 & \cdots & \mathbf{w}_{n-1} & \mathbf{w}_0 \end{bmatrix} \begin{bmatrix} a_0 \\ a_1 \\ \vdots \\ a_{n-1} \end{bmatrix},$$

where  $p_i$  are the unknown Bézier control points of patch  $P_i$ , and  $a_i$  the seven known vertices of the  $i^{th}$  two-ring section as labeled in Figure 3. Since this system is underdetermined, we introduce an energy functional and find the solution that minimizes this functional with respect to the constraints.

### 5. Bicubic Energy

Existing energy functionals, e.g. thin plate or biharmonics, have the disadvantage that they are not zero for bicubic surfaces. Our constraint system will be consistent with tensor product B-splines when  $n = 4$ . In order to generalize this case, we must define a new energy functional. We therefore introduce an energy functional, that to our knowledge has not previously appeared in the CAGD literature, whose absolute minimum of zero is achieved for a bicubic tensor product patch, and all higher degree parameterizations of such a patch.

Let  $F(u, v)$  be a tensor product patch. Our bicubic energy functional is defined as the integral

$$energy = \int_0^1 \int_0^1 \left( \frac{\partial^4}{\partial u^4} F(u, v) \right)^2 + \left( \frac{\partial^4}{\partial v^4} F(u, v) \right)^2 dudv.$$

In our case,  $F = P_i$  is a biseptic patch. Since the coefficients of  $P_i$  are at most squared, our energy functional can be written as a quadratic form

$$p_i^T E p_i,$$

where  $E$  is a symmetric  $64 \times 64$  matrix. Because  $\partial^4/\partial u^4$  and  $\partial^4/\partial v^4$  are identically zero for all bicubic patches, any vector  $p_i$  consistent with a bicubic patch (or a degree elevated form) will be in the kernel of  $E$ , implying  $p_i^T E p_i = E p_i = 0$ . We find the bicubic energy of the collection of patches  $P_i$  by the product  $\mathbf{p}^T \mathbf{E} \mathbf{p}$ , where  $\mathbf{E}$  is a block diagonal matrix whose  $n$  blocks are the single patch bicubic energy matrix  $E$ .

### 6. Constrained Minimization

We can minimize quadratic energy  $\mathbf{p}^T \mathbf{E} \mathbf{p}$  subject to constraints  $\mathbf{Cp} = \mathbf{W}\mathbf{a}$  using Lagrange multipliers. Differentiating with respect to  $\mathbf{p}$  yields

$$\frac{\partial}{\partial \mathbf{p}} (\mathbf{p}^T \mathbf{E} \mathbf{p}) = \frac{\partial}{\partial \mathbf{p}} (\mathbf{p}^T \mathbf{C}^T - \mathbf{a}^T \mathbf{W}^T) \Lambda, \\ 2\mathbf{E} \mathbf{p} = \mathbf{C}^T \Lambda.$$

These equations can be represented by a single block matrix

$$\begin{bmatrix} \mathbf{E} & \mathbf{C}^T \\ \mathbf{C} & \mathbf{0} \end{bmatrix} \begin{bmatrix} \mathbf{p} \\ \Lambda \end{bmatrix} = \begin{bmatrix} \mathbf{0} \\ \mathbf{W} \end{bmatrix} \mathbf{a}.$$

This system can be put into block circulant form by permuting its rows and columns to get

$$\begin{bmatrix} E & \mathbf{c}_0^T & 0 & 0 & \cdots & 0 & \mathbf{c}_1^T \\ \mathbf{c}_0 & 0 & \mathbf{c}_1 & 0 & & 0 & 0 \\ 0 & \mathbf{c}_1^T & E & \mathbf{c}_0^T & & \vdots & \vdots \\ 0 & 0 & \mathbf{c}_0 & 0 & & \vdots & \vdots \\ \vdots & & & & \ddots & 0 & 0 \\ 0 & 0 & \cdots & 0 & \mathbf{c}_1^T & E & \mathbf{c}_0^T \\ \mathbf{c}_1 & 0 & & 0 & 0 & \mathbf{c}_0 & 0 \end{bmatrix} \begin{bmatrix} p_0 \\ \lambda_0 \\ p_1 \\ \lambda_1 \\ \vdots \\ p_{n-1} \\ \lambda_{n-1} \end{bmatrix} = \begin{bmatrix} \mathbf{0} & \mathbf{0} & \cdots & \mathbf{0} \\ \mathbf{w}_0 & \mathbf{w}_1 & & \mathbf{w}_{n-1} \\ \mathbf{0} & \mathbf{0} & & \vdots \\ \mathbf{w}_{n-1} & \mathbf{w}_0 & & \vdots \\ \vdots & & \ddots & \mathbf{0} \\ \mathbf{0} & \cdots & \mathbf{0} & \mathbf{w}_1 \\ \mathbf{w}_1 & & \mathbf{w}_{n-1} & \mathbf{w}_0 \end{bmatrix} \begin{bmatrix} a_0 \\ a_1 \\ \vdots \\ a_{n-1} \end{bmatrix},$$

Rather than solving this  $119n \times 119n$  system directly, we transform the problem from the spatial to frequency domain by applying the Discrete Fourier Transform to the blocks. The Discrete Fourier Transform and Inverse Discrete Fourier Transform are given by

$$\hat{x}_j = \sum_{i=0}^{n-1} e^{\frac{2\pi\sqrt{-1}ij}{n}} x_i \quad \text{and} \quad x_i = \frac{1}{n} \sum_{j=0}^{n-1} e^{-\frac{2\pi\sqrt{-1}ij}{n}} \hat{x}_j.$$

We use the DFT to put the above system into block diagonal form, where the solution is found by solving the  $n$  individual  $119 \times 119$  blocks

$$\begin{bmatrix} E & \hat{\mathbf{c}}_j^H \\ \hat{\mathbf{c}}_j & \mathbf{0} \end{bmatrix} \begin{bmatrix} \hat{p}_j \\ \hat{\lambda}_j \end{bmatrix} = \begin{bmatrix} \mathbf{0} \\ \hat{\mathbf{w}}_j \end{bmatrix} \hat{a}_j,$$

for  $j = 0, \dots, n-1$ , where  $\hat{\mathbf{c}}_j^H$  denotes the conjugate transpose of  $\hat{\mathbf{c}}_j$ . The patch coefficients  $p_i$  are found by taking the IDFT of the solutions  $\hat{p}_j$ .

### 7. Basis Functions

To this point, we have assumed that the two-ring data  $a_i \in \mathbb{R}^m$  comes from a control mesh. If we let  $a_i$  take the form  $[0, \dots, 0, 1, 0, \dots, 0]$  then we are instead solving for the *basis function* associated with some  $a_i^{jk}$ , corresponding to the non-zero element. Since our constraint systems do not involve any actual data, only valence, we can solve for the

basis functions a priori, store the resulting basis patches and multiply them by local mesh data at runtime. Since a two-ring contains  $n$  sections of seven points, we only need to find seven basis functions for each valence  $n$ . We label these seven basis functions  $\mathbf{A}^{00}$ ,  $\mathbf{A}^{10}$ ,  $\mathbf{A}^{20}$ ,  $\mathbf{A}^{11}$ ,  $\mathbf{A}^{21}$ ,  $\mathbf{A}^{12}$ , and  $\mathbf{A}^{22}$ , where the indices correspond to the indices of  $a_i^{jk}$  to which they are associated.

An obvious question to ask about these basis function is: are they non-negative? By inspecting the Bernstein coefficients of the basis patches, we find the answer to be *no*, but just barely. There are a few negative coefficients on the order of  $10^{-3}$ , so this prevents us from claiming the *convex hull property*. We should point out that these negative values do not come from the external constraints; so a different (yet to be determined) energy functional could lead to the convex hull property. Alternatively, we could find the convex minimum to our constrained minimization problem; but this is complicated by the fact that we solve our system in the frequency domain, and convexity must be satisfied in the spatial domain. We leave this option for future work.

Another issue concerning the basis function is their support; that is, the collection of faces where a basis function non-zero. Presently, every basis function supported over an extraordinary vertex, will have support over all faces incident on that vertex. Ideally, the support of a basis function should not extend beyond the two-ring of its corresponding vertex. Otherwise, an extraordinary patch will depend on vertices outside the 1-ring of a quadrilateral face (i.e., vertices not connected by an edge to one of the quad face vertices). This extended support occurs for basis functions  $\mathbf{A}^{20}$ ,  $\mathbf{A}^{21}$ ,  $\mathbf{A}^{12}$ , and  $\mathbf{A}^{22}$ . Note that the patches outside the two-ring of the basis function are nearly zero, but not absolutely. We illustrate the point for the basis function  $\mathbf{A}^{21}$  in Figure 4. To deal with this issue, we enforce additional support constraints on patches associated with basis functions  $\mathbf{A}^{20}$ ,  $\mathbf{A}^{21}$ ,  $\mathbf{A}^{12}$ , and  $\mathbf{A}^{22}$ .

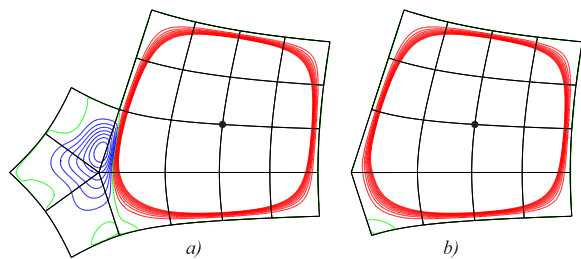


**Figure 4:** Contours from  $-1/2000$  to  $1/2000$  by  $1/20000$ . Red are positive contours, green zero, and blue negative. This basis function reaches a maximum height  $4/9$  at the solid dot, so the band of contours shown represents  $0.225\%$  of the height of the basis function. The basis function  $\mathbf{A}^{21}$  is shown a) without support constraints, and b) with support constraints

## 7.1. Support Constraints

To enforce ideal support we solve modified constraint systems. The cases of  $\mathbf{A}^{20}$ , and  $\mathbf{A}^{21}$  are similar; we treat  $\mathbf{A}^{12}$  as an instance of  $\mathbf{A}^{21}$  since they are the same up to diagonal reflection. In these cases, we want the basis functions to have support over two adjacent patches  $P_i(u, v)$  and  $P_{i+1}(u, v)$  incident on the extraordinary vertex. We impose external constraints 5, 6, and 7 on these two patches, as well as the internal geometric continuity constraints 8, 9, and 10 on the shared boundary  $P_i(0, t) = P_{i+1}(t, 0)$ . Next, we add constraints to force the basis function support boundary  $P_i(t, 0)$ , and  $P_{i+1}(0, t)$  to go to zero, along with all derivatives up to second order

$$\frac{\partial^k}{\partial v^k} P_i(t, 0) = 0, \quad \frac{\partial^k}{\partial u^k} P_{i+1}(0, t) = 0,$$

for  $k = 0, 1, 2$ . All patches other than  $P_i$  and  $P_{i+1}$  are set to zero. We then solve for minimum bicubic energy as before. Since we only need to solve for two patches, we do so in the spatial domain.

Enforcing two-ring support on the basis function  $\mathbf{A}^{22}$  is similar, except we only need to solve for a single patch. We use the external boundary constraints, along with constraints that force all derivatives up to second order along boundaries  $P_i(0, t)$  and  $P_i(t, 0)$  to zero.

Prior to enforcing the support constraints, the basis function were guaranteed to sum to 1 since the columns of the matrix  $\mathbf{W}$  in equation 11 sum to 1. Adding support constraints to select basis functions will cause this property to be violated. We can restore a partition of unity by simply defining

$$\mathbf{A}^{00} = 1 - \sum_{ijk} \mathbf{A}_{ijk}^i.$$

## 7.2. Boundary Basis Functions

Not all control meshes are closed. Frequently, artists model control meshes with boundary. For Catmull-Clark subdivision surfaces, the subdivision rules are modified so that the surface interpolates the cubic B-spline curve defined by the boundary edges [Nas87, BLZ00]. We can adapt this behavior to our surfaces by imposing mesh boundary constraints that force the surface to interpolate the boundary cubic B-spline curve.

We assume a boundary extraordinary vertex is surrounded by a *half two-ring* of mesh control points. We denote the valence of a boundary extraordinary vertex by  $m$ , the number of incident faces. We use the same correspondence maps as before, with the caveat that  $n = 2m$ .

First we need to modify the external boundary constraints to take into account the presence of a mesh boundary. We

define two bicubic patches

$$\bar{H}_0(u, v) = \mathbf{b}^3(u)^T \mathbf{M}^T \begin{bmatrix} a_2^{10} & a_1^{11} & a_1^{21} \\ a_0^{00} & a_1^{10} & a_1^{20} \\ a_0^{10} & a_0^{11} & a_0^{12} \\ a_0^{20} & a_0^{21} & a_0^{22} \end{bmatrix} \bar{\mathbf{M}} \mathbf{b}^3(v),$$

and

$$\bar{H}_{m-1}(u, v) = \mathbf{b}^3(u)^T \bar{\mathbf{M}}^T \begin{bmatrix} a_{m-2}^{10} & a_m^{00} & a_m^{10} & a_m^{20} \\ a_{m-2}^{11} & a_{m-1}^{10} & a_{m-1}^{11} & a_{m-1}^{12} \\ a_{m-2}^{12} & a_{m-1}^{20} & a_{m-1}^{21} & a_{m-1}^{22} \end{bmatrix} \mathbf{M} \mathbf{b}^3(v),$$

where

$$\bar{\mathbf{M}} = \frac{1}{6} \begin{bmatrix} 6 & 4 & 2 & 1 \\ 0 & 2 & 4 & 4 \\ 0 & 0 & 0 & 1 \end{bmatrix}.$$

We define two new mesh boundary constraints as

$$\begin{aligned} \frac{\partial^k}{\partial u^k} P_0(1, t) &= \frac{\partial^k}{\partial u^k} (\bar{H}_0 \circ \psi_n)(1, t), \\ \frac{\partial^k}{\partial v^k} P_{m-1}(t, 1) &= \frac{\partial^k}{\partial v^k} (\bar{H}_{m-1} \circ \psi_n)(t, 1), \end{aligned}$$

for  $k = 0, 1, 2$ . We use the external patch boundary constraints 5, 6 and 7 for boundaries  $P_0(t, 1)$  and  $P_{m-1}(1, t)$ , and for both external boundaries of patches  $P_i, i = 1, \dots, m-2$ . We include the internal geometric continuity constraints 8, 9, and 10 between pairs of patches  $P_i, P_{i+1}, i = 0, \dots, m-2$ . Finally, we include the boundary cubic B-spline constraints

$$\begin{aligned} P_0(t, 0) &= [a_m^{10} \ a_0^{00} \ a_0^{10} \ a_0^{20}] \cdot \mathbf{M} \cdot \mathbf{b}^3(t), \\ P_{m-1}(0, t) &= [a_0^{10} \ a_m^{00} \ a_m^{10} \ a_m^{20}] \cdot \mathbf{M} \cdot \mathbf{b}^3(t). \end{aligned}$$

We then solve to minimize bicubic energy as before.

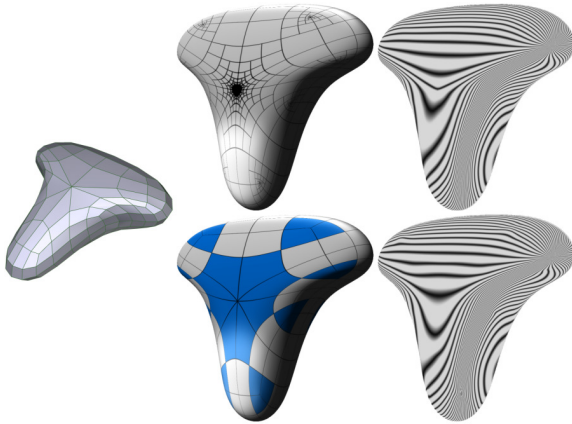


**Figure 5:** The control mesh, patch structures of the Catmull-Clark (top) and our surface (bottom) and the reflection lines. Notice that the valence 8 vertex from the Catmull-Clark surface causes a noticeable kink in the reflection lines that is absent with our  $G^2$  surface.

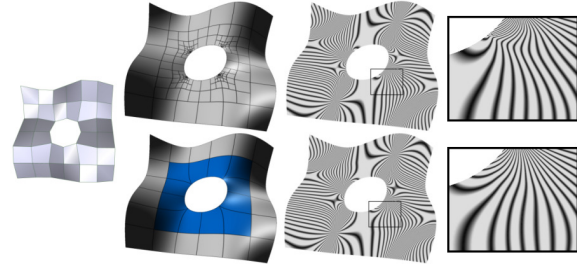


**Figure 6:** From left to right: the control mesh, the patch structure of a Catmull-Clark surface with bicubic patches shown in gray (top) and our surface with biseptric patches shown in blue (bottom), reflection lines and a zoom in close to an extraordinary boundary vertex. For the Catmull-Clark surface, we use the boundary rules of [BLZ00].

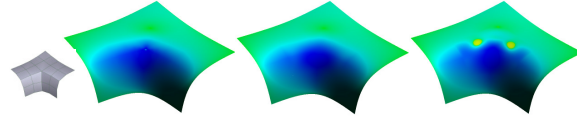


**Figure 7:** Comparison of Gaussian curvature for a Catmull-Clark surface (left), our technique (middle) and [Loo04] (right).

## 8. Results

We show several examples of our surfaces in figures 5 to 11. The quality of our shapes is quite good in general compared with Catmull-Clark subdivision, especially near boundary and high valence extraordinary vertices. One issue that we have noticed are curvature ‘hotspots’, high positive Gauss curvature, for valence  $n = 3$ ; similar to the behavior of Catmull-Clark surfaces. We have not treated this as a special case in anyway; though doing so may result in better shapes. The lack of a convex hull property warrants additional work on this scheme.

## References

- [ADS06] AUGSDÖRFER U., DODGSON N., SABIN M.: Tuning subdivision by minimising gaussian curvature variation near extraordinary vertices. *Computer Graphics Forum* 25, 3 (2006), 263–272. 1
- [BLZ00] BIERMANN H., LEVIN A., ZORIN D.: Piecewise smooth subdivision surfaces with normal control. In *SIGGRAPH '00: Proceedings of the 27th annual conference on Computer graphics and interactive techniques* (2000), pp. 113–120. 7
- [CC78] CATMULL E., CLARK J.: Recursively generated B-spline surfaces on arbitrary topological meshes. *Computer Aided Design* 10, 6 (1978), 350–355. 1
- [DeR85] DEROSE A.: *Geometric Continuity: A Parametrization Independent Measure of Continuity for Computer Aided Geo-*

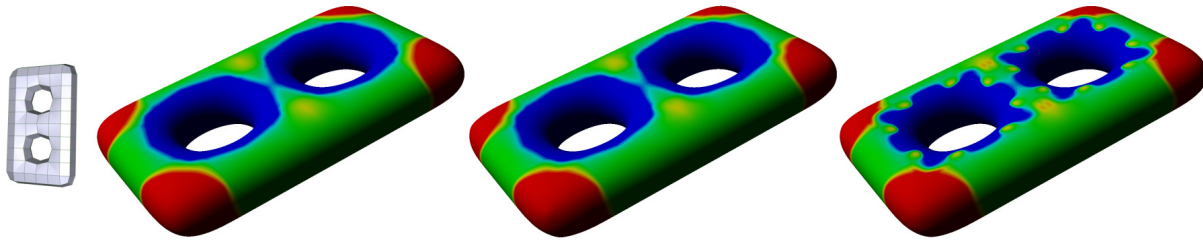


**Figure 8:** Comparison of Gaussian curvature for a Catmull-Clark surface (left), our technique (middle) and [Loo04] (right).

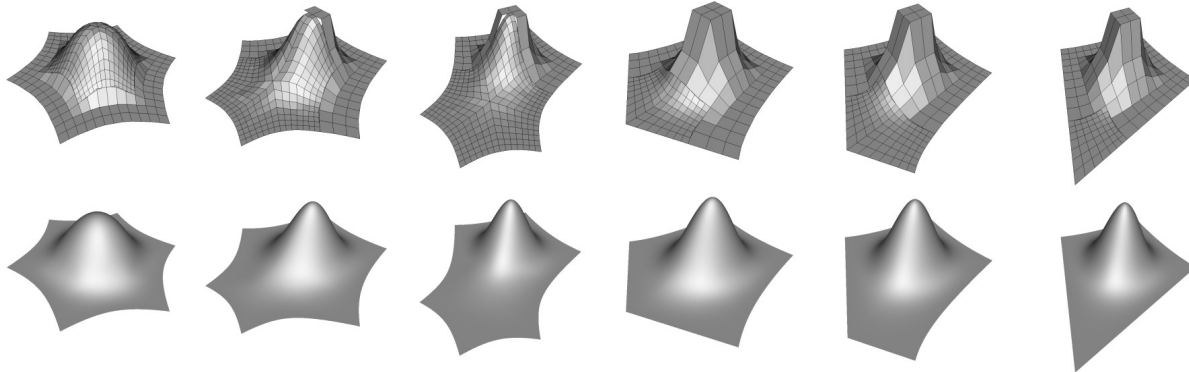


**Figure 9:** Plots of the basis functions we compute for a valence 6 vertex. The Bezier nets (top row) of the basis functions (bottom row) are composed of bicubic polynomials in the two-ring of an extraordinary vertex and biseptic patches in the one-ring.

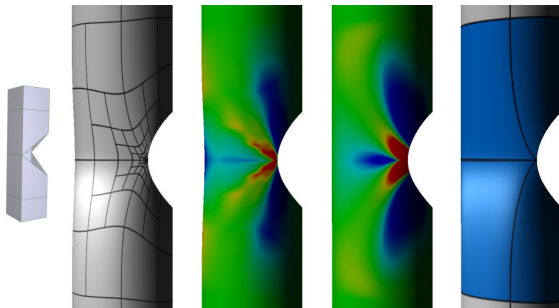


**Figure 10:** Gaussian curvature plots of a boundary vertex with four quads for a Catmull-Clark surface (left) and our technique (right).

*metric Design*. PhD thesis, Berkeley, 1985. also tech report UCB/CSD 86/255. 2

- [DS78] DOO D., SABIN M.: Behaviour of recursive division surfaces near extraordinary points. *Computer Aided Design* 10, 6 (1978), 356–360. 1
- [GU07] GINKEL I., UMLAUF G.: Tuning subdivision algorithms using constrained energy minimization. In *Mathematics of Surfaces XII* (2007), Martin R., Sabin M., Winkler J., (Eds.), Springer-Verlag, pp. 166–176. 1

- [GZ99] GREGORY J., ZHOU J.: Irregular  $C^2$  surface construction using b-polynomial rectangular patches. *Computer Aided Geometric Design* 16, 5 (1999), 423–435. 2
- [Hah89] HAHN J.: Geometric continuous patch complexes. *Computer Aided Geometric Design* 6, 1 (1989), 55–68. 3
- [HKD93] HALSTEAD M., KASS M., DEROSE T.: Efficient, fair interpolation using catmull-clark surfaces. *Computer Graphics* 27, Annual Conference Series (1993), 35–44. 2
- [KP07] KARCIAUSKAS K., PETERS J.: Guided  $C^2$  spline surfaces with v-shaped tessellation. In *IMA Conference on the Mathematics of Surfaces* (2007), pp. 233–244. 2
- [Lev06] LEVIN A.: Modified subdivision surfaces with continuous curvature. *Computer Graphics* 25, Annual Conference Series (2006), 1035–1040. 1
- [Loo04] LOOP C.: Second order smoothness over extraordinary vertices. In *Proceedings of the Symposium on Geometry Processing* (2004), pp. 169–178. 2, 3, 8
- [Nas87] NASRI A. H.: Polyhedral subdivision methods for free-form surfaces. *ACM Trans. Graph.* 6, 1 (1987), 29–73. 1, 7
- [Pet02] PETERS J.:  $C^2$  free-form surfaces of degree (3,5). *Computer Aided Geometric Design* 19, 2 (2002), 113–126. 2
- [PR98] PETERS J., REIF U.: Analysis of generalized B-spline subdivision algorithms. *SIAM Journal on Numerical Analysis* 35, 2 (Apr. 1998), 728–748. 1
- [Pra97] PRAUTZSCH H.: Freeform splines. *Computer Aided Geometric Design* 14, 3 (1997), 201–206. 2

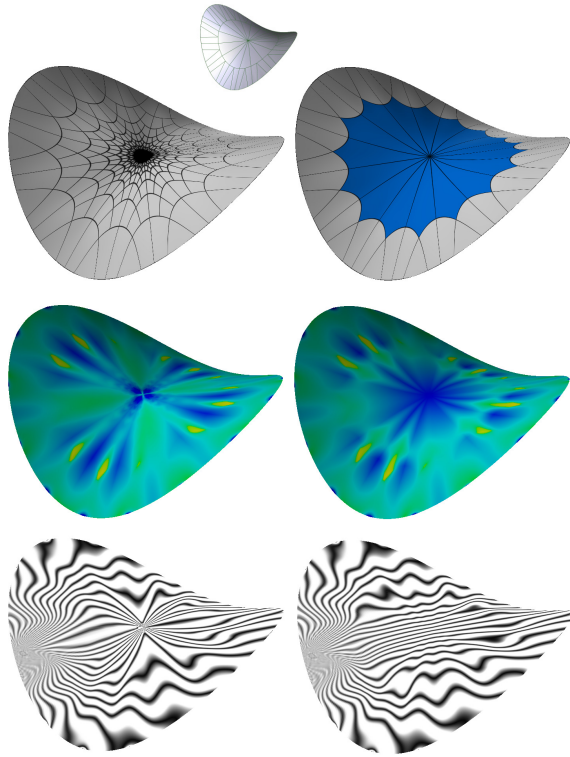


**Figure 11:** Comparison of a valence 17 vertex for Catmull-Clark surface (left), and our technique (right). Below control mesh: (top row) patch structure, (middle row) Gaussian curvature, and (bottom row) reflection lines.

[Pra98] PRAUTZSCH H.: Smoothness of subdivision surfaces at extraordinary points. *Advances in Computational Mathematics* 9 (1998), 377–390. 1

[PU98] PRAUTZSCH H., UMLAUF G.: A  $G^2$ -subdivision algorithm. In *Geometric Modelling, volume 13 of Computing suppl* (1998), G. Farin H. Bieri G. B., DeRose T., (Eds.), Springer-Verlag. 1

[Rei95] REIF U.: A unified approach to subdivision algorithms near extraordinary vertices. *Computer Aided Geometric Design* 12 (1995), 153–174. 1

[Rei98] REIF U.: Turbs – topologically unrestricted rational b-splines. *Constructive Approximation* 14, 1 (1998), 57–77. 1

[RS99] REIF U., SCHRÖDER P.: *Curvature smoothness of subdivision surfaces*. Tech. Rep. TR-00-03, Caltech, 1999. 1

[Sab91] SABIN M.: Cubic recursive division with bounded curvature. In *Curves and Surfaces* (1991), Laurent P., Méhauté A. L., Schumaker L., (Eds.), Academic Press, pp. 411–414. Boston. 1

[Sta98] STAM J.: Exact evaluation of Catmull-Clark subdivision surfaces at arbitrary parameter values. *Computer Graphics* 32, Annual Conference Series (1998), 395–404. 2

[Zor06] ZORIN D.: Constructing curvature-continuous surfaces by blending. In *SGP '06: Proceedings of the fourth Eurographics*

*symposium on Geometry processing* (2006), Eurographics Association, pp. 31–40. 1

### Appendix A: Solving for $\psi_n$

We now use the constraints implied by the cocycle conditions on vertices to solve for a mapping  $\psi_n$  that will minimize the bidegree of our  $G^2$  surface spline. In the  $G^2$  case, the cocycle condition must hold for all second order mixed partial derivatives. In general, the  $k^{th}$  order derivatives will transform via Equation 1 in terms of all  $k^{th}$  order derivatives of the correspondence maps. However at type 2 and 3 vertices this is not the case since at these 4-valent vertices, various mixed partial derives of the mappings  $\phi_n$  and  $\psi_n$  vanish. Therefore, the matrices in Equations 3 and 4 are  $8 \times 8$  and contain the derivatives:

$$\frac{\partial}{\partial u}, \frac{\partial}{\partial v}, \frac{\partial^2}{\partial u^2}, \frac{\partial^2}{\partial u \partial v}, \frac{\partial^2}{\partial v^2}, \frac{\partial^3}{\partial u^2 \partial v}, \frac{\partial^3}{\partial u \partial v^2}, \frac{\partial^4}{\partial u^2 \partial v^2}.$$

Specifically, let

$$\Psi_n = \begin{bmatrix} 1 & 0 & 0 & x_{11} & 0 & x_{21} & x_{12} & x_{22} \\ 0 & 1 & 0 & y_{11} & 0 & y_{21} & y_{21} & y_{22} \\ 0 & 0 & 1 & 0 & 0 & 2x_{11} & 0 & 2x_{11}^2 + 2x_{12} \\ 0 & 0 & 0 & 1 & 0 & 2y_{11} & 2x_{11} & 2x_{21} + 4x_{11}y_{11} + 2y_{21} \\ 0 & 0 & 0 & 0 & 1 & 0 & 2y_{11} & 2y_{11}^2 + 2y_{21} \\ 0 & 0 & 0 & 0 & 0 & 1 & 0 & 4x_{11} \\ 0 & 0 & 0 & 0 & 0 & 0 & 1 & 4y_{11} \\ 0 & 0 & 0 & 0 & 0 & 0 & 0 & 1 \end{bmatrix},$$

where  $x_{ij} = \frac{\partial^{i+j}}{\partial u^i \partial u^j} \psi_{n,x}(1, 0)$ . While  $y_{ij}$  can be defined similarly, we note that since (by assumption) the  $x$  and  $y$  components of  $\psi_n$  are symmetric, that is  $\psi_{n,x}(v, u) = \psi_{n,y}(u, v)$ , we need only solve for  $\psi_{n,x}$ . Therefore  $y_{ij} = \frac{\partial^{i+j}}{\partial u^i \partial u^j} \psi_{n,x}(0, 1)$ . Multiplying together the matrices in Equation 3 leads to the following four constraints on  $\psi_{n,x}$

$$\begin{aligned} x_{11} &= -c_n, & x_{21} &= 0, \\ y_{12} &= -2c_n(y_{11} + c_n), & y_{22} &= -2c_n(2y_{21} - y_{12}). \end{aligned}$$

It is possible to satisfy these constraints with a bidegree 3 mapping; with this solution, the derivative  $\frac{\partial}{\partial u} \psi_{n,x}(1, v)$  will be degree 3. This term gets squared under the chain rule leading to higher degree surfaces than necessary. Instead we can satisfy the above constraints with a bidegree  $4 \times 3$  polynomial, leaving additional freedom to lower the overall surface degree. We can write this polynomial  $\psi_{n,x}(u, v) =$

$$\mathbf{b}^A(u)^T \begin{bmatrix} 0 & 0 & 0 & 0 \\ \frac{1}{4} & \frac{c_n(c_n^2(7c_n+6)-18(c_n+2)\alpha)+27}{12(c_n-3)(2c_n-3)} & \frac{c_n^2+3c_n-18\alpha}{12(c_n-3)} & \frac{1}{4} \\ \frac{1}{4} & \frac{c_n+3}{6} & \alpha & \frac{1}{4} \\ \frac{1}{4} & \frac{c_n+9}{12} & \beta & \frac{1}{4} \\ 1 & 1 & 1 & 1 \end{bmatrix} \mathbf{b}^B(v).$$

We now solve for the 2 degrees of freedom  $\alpha$  and  $\beta$  so that  $\frac{\partial}{\partial u} \psi_{n,x}(1, v)$  is degree 2 and  $\frac{\partial}{\partial v} \psi_{n,x}(u, 1)$  is degree 3. These constraints result in

$$\alpha = \frac{c_n^2+3c_n-9}{9(c_n-2)}, \quad \beta = \frac{9+c_n}{12}.$$

As shown in a Section 4.1, the bidegree of the resulting surfaces are minimized.